ACS OMEGA

http://pubs.acs.org/journal/acsodf

Article

Study on the Preparation of Nano-FeS Loaded on Fly Ash and Its Cr Removal Performance

Xuying Guo,* Zhiyong Hu, Xinle Gao, Yanrong Dong, and Saiou Fu

Cite This: *ACS Omega* 2022, 7, 32331−32338

Read Online

ACCESS | Metrics & More | Article Recommendations

ABSTRACT: Chromium has been considered as one of the most hazardous heavy metals because of its strong and persistent toxicity to the ecosystem and human beings. In this study, fly ash-loaded nano-FeS (nFeS-F) composites were constructed with fly ash as the carrier, and the performance and mechanism of the composites for the removal of Cr(VI) and total chromium from water were investigated. The composite was characterized by X-ray diffraction and transmission electron microscopy. The effects of fly ash size, molarity of $FeSO_4$, and flow rate of $FeSO_4$ solution on the removal of Cr(VI) and total chromium were investigated by a single factor experiment. The interaction of various factors was studied by the Box-Behnken response surface methodology. The optimum conditions of removal of Cr(VI)and total chromium by nFeS-F were determined. The results show that ① the optimal preparation conditions for nFeS-F were an $FeSO_4$ concentration of 0.45 mol/L, a fly ash particle size of 120−150 mesh, and a flow rate of 0.43 mL/s.② The response surface model provides reliable predictions for the removal efficiencies of Cr(VI) and total chromium.③ The removal efficiencies of Cr(VI) and total chromium were 92.87 and 83.53%, respectively, under the optimal preparation conditions by the experimental test. This study provides an effective method for the removal of Cr(VI) and total chromium.

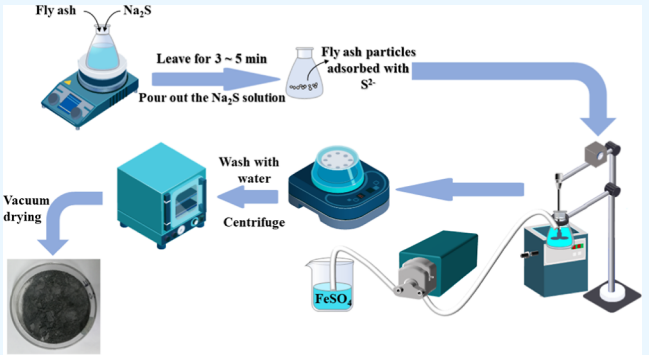

1. INTRODUCTION

With the development of modern industry, a large amount of chromium-containing wastewater inevitably enters the water and soil environment, endangering human health. Chromium often exists in water bodies in the state of Cr(III) and Cr(VI), which is highly toxic, difficult to degrade, and difficult to treat.[1,2] Currently, the commonly used treatment methods are adsorption,[3] ion exchange,[4] electrochemical,[5] and reduction precipitation.[6] The reduction precipitation method is widely used to treat highly concentrated acidic chromium-containing wastewater because of its easy operation, stable operation, and low price.[7]

Nano FeS has good adsorption performance, efficient reduction ability, large surface area, and high reactivity, which is considered as an efficient material for treating chromium pollution.[8] Li et al.[9] used a homogeneous precipitation method to prepare FeS nanoparticles to remove Cr(VI) from soil, and the removal rate of Cr(VI) was as high as 98% at a molar ratio of FeS to Cr(VI) of 1.5:1. Due to the high surface energy and susceptibility to oxidative agglomeration of nano-FeS, there is a need to provide a carrier material that enhances its stability.[10] Yao et al.[11] used a novel colloid of polyacrylate compounded with nano-FeS to remove Cr(VI) from water, which improved the dispersion and stability of nano-FeS by increasing the spatial site resistance and electrostatic repulsion between nano-FeS particles. Park et al.[12] used experiments to compare the adsorption capacity of quartz sand for Cr(VI) before and after loading FeS, and the results showed that the adsorption of Cr(VI) by quartz sand after loading FeS was 25.2 times higher than that of quartz sand. The research group[13] achieved better results using lignite loaded with nano-FeS to treat acidic chromium-containing wastewater in the previous stage. However, the high cost of lignite is not suitable for large-scale application. Therefore, further screening of cheap and stable carrier materials is needed.

Fly ash, as an industrial waste, is produced in China alone at more than 600 million tons per year.[14,15] Because of its good physicochemical properties such as high porosity and large surface area, it is often used as an adsorbent to treat wastewater.[16−18] Ribeiro et al.[19] used fly ash after gasification for the adsorption of Cr(VI), and the results showed that fly

Received: June 14, 2022
Accepted: August 10, 2022
Published: September 2, 2022

Table 1. Main Composition of Fuxin Fly Ash

constituent	SiO_2	TiO_2	Al_2O_3	Fe_2O_3	MnO	MgO	CaO	Na_2O	K_2O	P_2O_5
fly ash	67.10	0.12	19.74	3.35	0.34	2.87	4.00	1.08	1.30	0.10

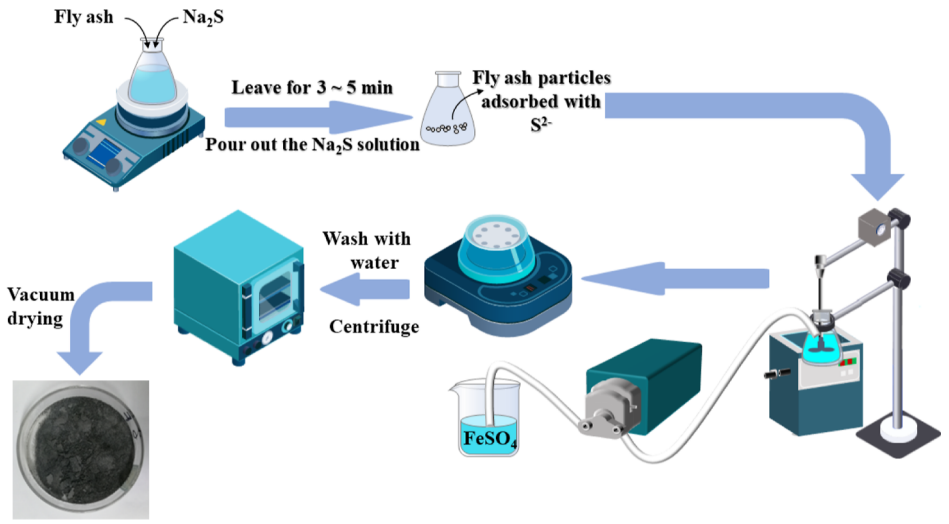

Figure 1. Flow chart of the preparation of nFeS-F.

ash has the potential to be a cheap and effective adsorbent. Wang et al.[20] investigated the adsorption characteristics of fly ash on Cr(VI) through intermittent experiments, and the experimental results showed that the initial concentration of Cr(VI) was 10 mg/L, and the removal rate of Cr(VI) was only 50.13%. Li et al.[21] treated chromium-containing wastewater with fly ash modified by polymeric aluminum chloride, and the Cr(VI) removal rate reached 80.2%. Chen[22] loaded iron-based nanomaterials onto the surface of fly ash by an in situ reduction method, which effectively enhanced the removal capacity of fly ash for Cr(VI).

Based on this, the author considered the use of fly ash loaded with nFeS for the treatment of acidic chromium-containing wastewater, which can solve the technical bottleneck of the small adsorption capacity of fly ash and the easy agglomeration of nFeS and ensure the adsorption of fly ash and the advantages of nFeS redox in the treatment of acidic chromium-containing wastewater to be maximized. The effects of fly ash particle size, the molarity of $FeSO_4$, and the flow rate on the treatment of chromium-containing wastewater with nFeS-F were investigated by the response surface methodology (RSM)[23] to determine the optimal preparation conditions. The aim is to provide a theoretical basis for the treatment of acidic chromium-containing wastewater with fly ash-loaded FeS.

2. MATERIALS AND METHODS

2.1. Experimental Materials. Fly ash was collected from the Fuxin coal-fired power plant in Liaoning Province, China; it is new fly ash. The formation of fly ash is divided into three stages: ① pulverized coal → porous carbon particles. ② Porous carbon particles → porous vitreous body. ③ Porous vitreous body → glass beads. The main chemical composition of fly ash is shown in Table 1. All chemicals were purchased from Sinopharm Chemical Reagent Co., Ltd. All the chemicals selected for the experiments were of analytical reagent grade. Deionized water was always used to prepare the required solutions.

Acidic chromium-containing wastewater: the pH of the simulated acid mine wastewater was set to 4, and the mass concentration of Cr(VI) was 100 mg/L.

2.2. Preparation of Composite Adsorbent nFeS-F. 4 g of fly ash and 60 g of Na_2S were placed in a conical flask, water was added, and the mixture was stirred for 8 h and set aside. The 0.45 mol/L $FeSO_4$ solution was added dropwise (0.45 mL/s) to the conical flask with a peristaltic pump, sonicated (40 kHz) for 10 min, and the suspension was poured into a centrifuge tube, centrifuged for 15 min, and washed of impurities, and the result was the new composite adsorbent material of nFeS-F. After vacuum drying, it was sealed and stored. The nFeS-F preparation process is shown in Figure 1.

2.3. Single Factor Test. The single factor method was used to investigate fly ash particle sizes (30−60, 60−90, 90−120, 120−150, and 150−180 mesh), molarities of $FeSO_4$ (0.15, 0.3, 0.45, 0.6, and 0.75 mol/L), and flow rate of $FeSO_4$ solution (0.33, 0.43, 0.53, 0.63, and 0.73 mL/s) of nFeS-F on the treatment of acidic chromium-containing wastewater. The nFeS-F was injected into the acidic chromium-containing wastewater at a solid−liquid ratio of 1:200 (g/mL), shaken at 300 rpm, and sampled at regular intervals. Each experiment was repeated three times. Based on the evaluation indexes of Cr(VI) and total chromium removal efficiencies, the optimal preparation conditions of the new nFeS-F composite adsorbent were determined.

2.4. Response Surface Test. Based on the single factor experiment, three levels of the three factors of molarity of $FeSO_4$, fly ash particle size, and flow rate of $FeSO_4$ solution were selected as the response surface optimization design. The labels and level of test factors are shown in Table 2.

2.5. Water Quality Testing Method. The determination of Cr(VI) in water samples was performed by the diphenylcarbazide spectrophotometry (GB/T 7467-1987) at a wavelength of 540 nm; the total chromium was determined by potassium permanganate oxidation-diphenylcarbazide spectrophotometry (GB/T 7466-1987), measured at a wavelength of 540 nm.

https://doi.org/10.1021/acsomega.2c03699
ACS Omega 2022, 7, 32331−32338

Table 2. Level of Impact Factors and Labels

factor	labels	level −1	level 0	level 1
fly ash particle size (mesh)	X_1	100	130	160
molarity of $FeSO_4$ (mol/L)	X_2	0.3	0.45	0.6
flow rate of $FeSO_4$ solution (mL/s)	X_3	0.43	0.53	0.63

3. EXPERIMENTAL RESULTS AND DISCUSSION

3.1. XRD and TEM Analysis. The X-ray diffraction (XRD) and transmission electron microscopy (TEM) characterization results of nFeS-F samples and fly ash samples are shown in Figure 2.

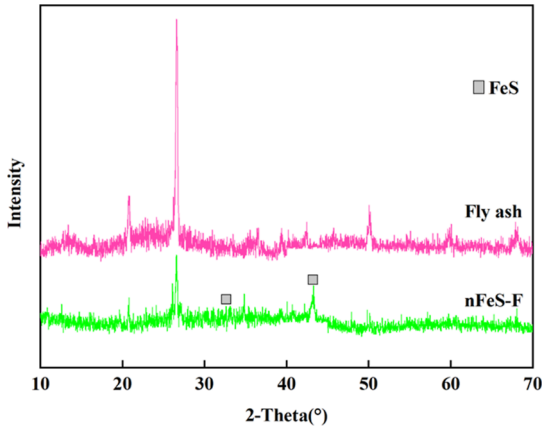

Figure 2. XRD patterns of fly ash and nFeS-F.

It can be seen from Figure 2 that the loaded nFeS-F has characteristic diffraction peaks at 2θ = 20.85, 26.62, 50.11, and 68.10°, indicating that the loading of nano-FeS does not change the original crystal structure of fly ash. FeS diffraction peaks (PDF: # 76-0963) appeared at 2θ = 32.68 and 43.17° of nFeS-F after loading, which indicated that FeS was successfully loaded on the surface of fly ash. As shown in Figure 3, the FeS

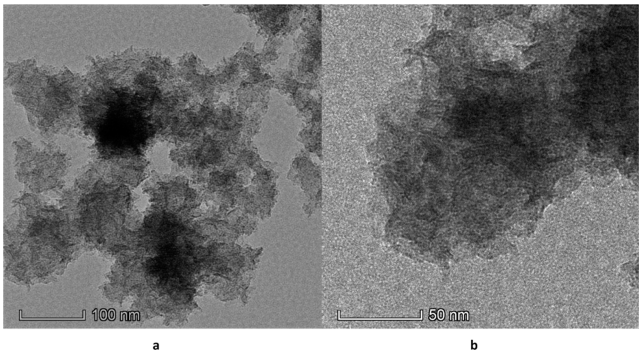

Figure 3. TEM image of nFeS-F. (a) 100 and (b) 50 nm.

crystals loaded on the surface of fly ash are sheet-like with an average length of 40−80 nm, and the morphology is similar to the nano-FeS prepared by Dai,[24] indicating that the ultrasonic precipitation method can load the nano-FeS on fly ash particles.

Nanoparticles are uniformly distributed in nFeS-F with good dispersion, which shows that fly ash as a carrier material can effectively improve the stability of nano-FeS and inhibit the condensation and agglomeration of nano-FeS itself.

3.2. Single Factor Test Analysis. *3.2.1. Effect of Fly Ash Particle Size on Chromium Removal Efficiency.* The effect of fly ash particle size on the removal efficiency of Cr(VI) and total chromium is shown in Figure 4. With the decrease of fly ash particle size, the removal efficiency of Cr(VI) and total chromium by nFeS-F showed a trend of increasing and then decreasing. The removal of Cr(VI) and total chromium reached a maximum of 92.09 and 80.27% at a fly ash particle size of 120−150 mesh. This is due to the decrease in fly ash particle size and increase in specific surface area, which enhances the adsorption capacity of chromium.[25] At the same time, the specific surface area of fly ash increases and the adsorption sites gradually increase, making fly ash loaded with more FeS.

The results showed that the adsorption of Cr(VI) by nFeS-F consumes H^+, and the surface of nFeS-F is positively charged, and so, the removal efficiency of Cr(VI) is improved by charge adsorption.[26] When the particle size of fly ash is too small, the prepared nFeS-F is easy to float on the water surface and difficult to settle in the process of treating chromium-containing wastewater, and so, the removal effect will be affected. Therefore, 120−150 mesh was selected as the fly ash particle size in the follow-up experiment.

3.2.2. Effect of the Molarity of $FeSO_4$ on Chromium Removal Efficiency. The effect of the molarity of $FeSO_4$ on the removal efficiency of Cr(VI) and total chromium is shown in Figure 5. When the molarity of $FeSO_4$ was 0.45 mol/L, the removal efficiency rates of Cr(VI) and total chromium reached the maximum, which were 92.58 and 82.99%, respectively. This is because the concentration of $FeSO_4$ solution has great influence on the nucleation and growth rate of crystals. When the concentration of Fe^{2+} ions in solution increases, the number of FeS crystals increases. With the increase of $FeSO_4$ molarity, many tiny grains can provide larger collision area and more active sites, and so, the removal efficiency of Cr(VI) and total chromium increases.[27] The molarity of $FeSO_4$ continued to increase, but the removal efficiency of Cr(VI) and total chromium did not increase significantly, which indicated that the molarity of Fe^{2+} in the solution had tended to be saturated. Therefore, 0.45 mol/L was selected as the molarity of $FeSO_4$ in the follow-up experiment.

3.2.3. Effect of the Flow Rate on Chromium Removal Efficiency. The effect of flow rate on the Cr(VI) and total chromium removal efficiency is shown in Figure 6. It can be seen from Figure 6 that with the acceleration of the drop addition flow rate, nFeS-F showed a trend of increasing and then decreasing the removal efficiency of Cr(VI) and total chromium. When the flow rate of $FeSO_4$ solution was 0.33 mL/s, the removal efficiency rates of Cr(VI) and total chromium reached the maximum, which were 89.15 and 79.68%, respectively. It is due to the fact that the dropwise flow rate of the solution affects the crystal structure of FeS, and the supersaturated nucleation and growth rate theory of Weinman[28] demonstrated that the dropwise flow rate is proportional to the nucleation and growth rates of FeS crystals.

When the flow rate of $FeSO_4$ solution is small, the grain size of the nuclei is small and the surface free energy is high, which makes the removal efficiency of Cr(VI) and total chromium the highest. As the flow rate of $FeSO_4$ solution increases, the crystal size increases rapidly and the specific surface area decreases, leading to a decrease in the removal efficiency of

https://doi.org/10.1021/acsomega.2c03699
ACS Omega 2022, 7, 32331−32338

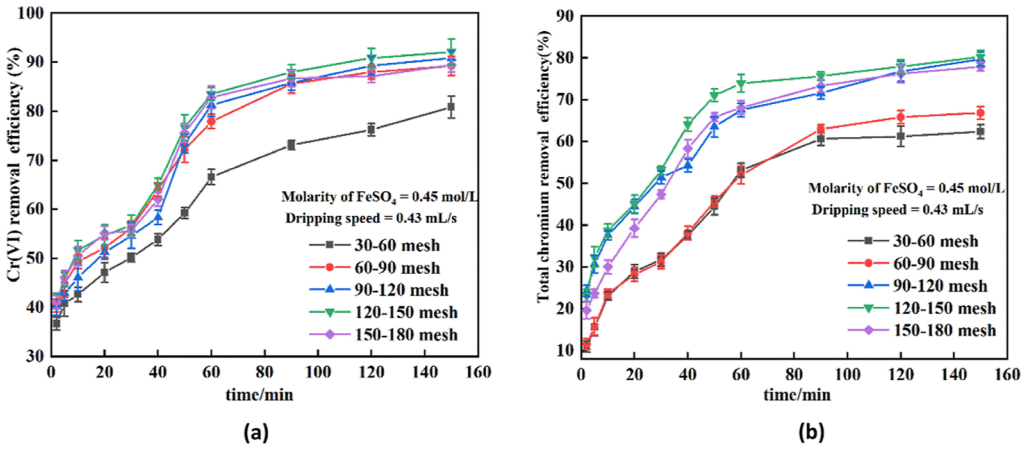

Figure 4. Effect of fly ash particle size on the removal efficiency of Cr(VI) and total chromium. (a) Cr(VI) removal efficiency (%). (b) Total chromium removal efficiency (%).

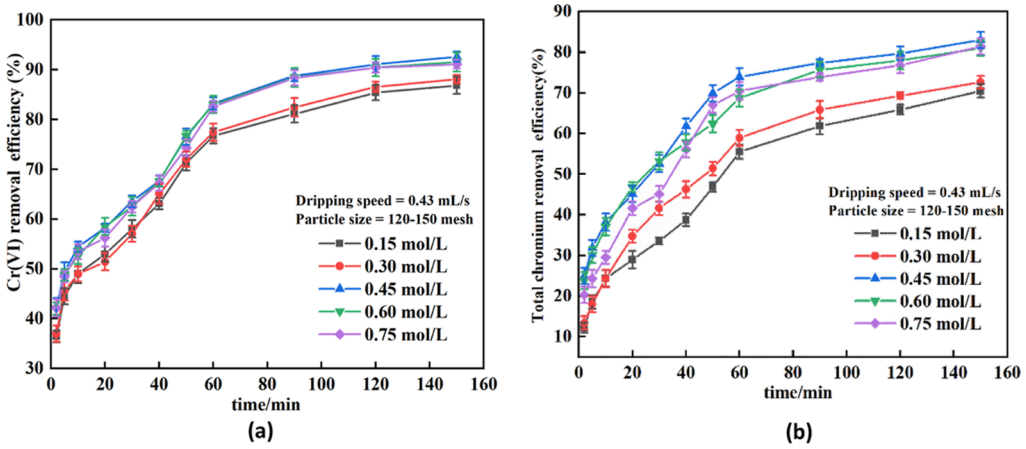

Figure 5. Effects of molarity of $FeSO_4$ on the removal efficiency of Cr(VI) and total chromium. (a) Cr(VI)removal efficiency (%). (b) Total chromium removal efficiency (%).

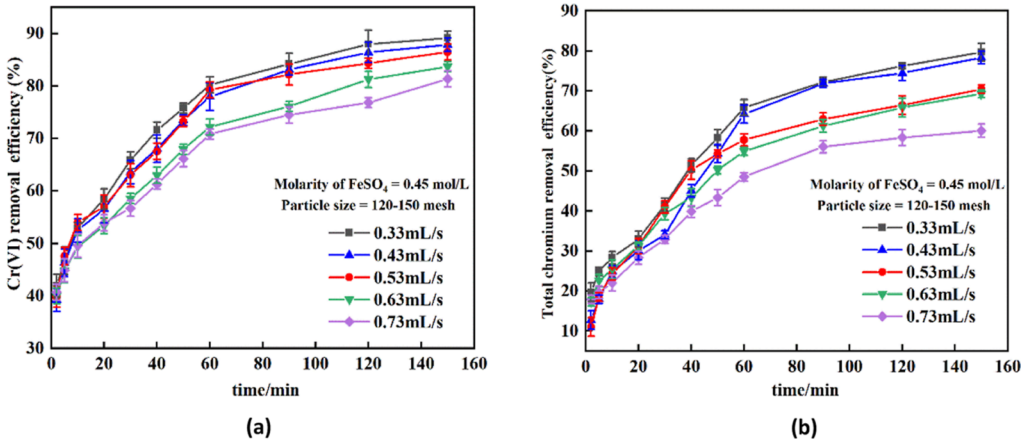

Figure 6. Flow rate of $FeSO_4$ solution on the removal efficiency of Cr(VI) and total chromium. (a) Cr(VI) removal efficiency (%). (b) Total chromium removal efficiency (%).

Cr(VI) and total chromium. At the same time, the concentration of Fe^{2+} ions constituting FeS crystals in solution increases, the rate of grain formation is accelerated, and the number of crystals increases. After comprehensive consideration, 0.43 mL/s was selected as the flow rate of $FeSO_4$ solution in the follow-up experiment.

3.3. Response Surface Test Analysis. RSM is an experimental condition finding method for solving problems related to nonlinear data processing.[29] Box-Behnken design is one of the common experimental design methods used in response surface optimization.[30] This method performs response surface analysis on the experimentally derived data results to obtain a prediction model. The prediction model is

https://doi.org/10.1021/acsomega.2c03699
ACS Omega 2022, 7, 32331−32338

continuous and generally curved. The advantage is that the experimental parameters can be analyzed continuously at each level during the experimental parameter optimization. The experiment considered three factors: fly ash particle size, molarity of $FeSO_4$, and flow rate, and the degree of their effects on the removal rates of Cr(VI) and total chromium were obtained by interaction experiments. In accordance with the statistical requirements of the Box-Behnken experimental design, 17 sets of experimental regression coefficients were fitted to the equations, and the results are shown in Tables 3−5. The calculation formula is

$$Y = \beta_0 + \beta_1 A + \beta_2 B + \beta_3 C + \beta_{11} A^2 + \beta_{22} B^2 + \beta_{33} C^2 + \beta_{12} AB + \beta_{13} AC + \beta_{23} BC$$

Table 3. Experimental Design Factors and Results[a]

code	X_1	X_2	X_3	total chromium removal efficiency (%)	Cr(VI) removal efficiency (%)
1	0.60	160.00	0.53	78.62	88.52
2	0.45	100.00	0.43	72.22	90.04
3	0.30	160.00	0.53	83.42	87.24
4	0.60	100.00	0.53	70.65	82.52
5	0.45	130.00	0.53	81.22	90.53
6	0.45	130.00	0.53	81.20	90.52
7	0.45	130.00	0.53	81.23	90.48
8	0.45	100.00	0.63	76.52	93.82
9	0.45	130.00	0.53	81.24	90.53
10	0.60	130.00	0.63	76.92	86.68
11	0.60	130.00	0.43	71.23	84.21
12	0.45	160.00	0.43	79.32	92.42
13	0.45	160.00	0.63	87.62	94.32
14	0.30	130.00	0.63	80.96	90.12
15	0.45	130.00	0.53	81.22	90.54
16	0.30	100.00	0.53	76.62	87.32
17	0.30	130.00	0.43	78.02	87.52

[a]Notes: X_1 is the molarity of $FeSO_4$, mol/L; X_2 is the size of fly ash, mesh; and X_3 is the flow rate of $FeSO_4$ solution, mL/s.

where y is the predicted corresponding value, A, B, and C are the coded values of the independent variables, and β is the constant term.

According to the experimental results of response surface design in Table 3, a quadratic polynomial model between fly ash particle size, $FeSO_4$ molarity, flow rate of $FeSO_4$ solution, and Cr(VI)and total chromium removal efficiencies was established. The regression equation of Cr(VI) removal efficiency is as follows: $Y = 90.52 - 1.28A + 1.10B + 1.34C + 1.52AB - 0.032AC - 0.47BC - 4.82A^2 + 0.70B^2 + 1.43C^2$; the regression equation of total chromium removal efficiency is as follows: $Y = 81.22 - 2.70A + 4.12B + 2.65C + 0.29AB + 0.69AC + 1.00BC - 3.02A^2 - 0.88B^2 - 1.42C^2$, where A represents the molarity of $FeSO_4$, mol/L; B represents the size of fly ash, mesh; and C represents the flow rate of $FeSO_4$ solution, mL/s. It can be seen from Tables 4 and 5 that the p values of the regression model of Cr(VI) and total chromium removal efficiencies are both <0.0001, indicating that the model is extremely significant; p values of misfit terms are all >0.05, and it shows that the model fits well with the experiment, and the regression equation can be used to analyze the experimental results instead of the real points. The correction determination

Table 4. Variance Analysis Table of Second-Order Model of Cr(VI) Removal Efficiency

variance source	sum of squares	degree of freedom	mean square	F-value	p-value
model	152.16	9	16.90	47.18	<0.0001
A-molarity of $FeSO_4$	13.18	1	13.18	36.79	0.0005
B-the size of fly ash	9.68	1	9.68	27.01	0.0013
C-the flow rate of $FeSO_4$ solution	14.44	1	14.44	40.31	0.0004
AB	9.24	1	9.24	25.79	0.0014
AC	0.01	1	0.01	0.011	0.9166
BC	0.88	1	0.88	2.46	0.1603
A^2	97.76	1	97.76	272.87	<0.0001
B^2	2.05	1	2.05	5.73	0.0478
C^2	8.62	1	8.62	24.07	0.0017
residual error	2.50	7	0.35		
degree of misfit	2.50	3	0.83	151.86	0.0658
pure error	0.0022	4	0.00055		
total deviation	154.67	16			

coefficients R^2_{adj} of the two models were 0.9629 and 0.9750, respectively, indicating that 3.71 and 2.5% of the variance, respectively, could not be explained by the model.[31] The coefficients of variation were 0.67 and 0.89, respectively, which further indicated that the model was accurate and suitable for preliminary analysis and prediction of Cr(VI) and total chromium removal efficiency.

3.3.1. Cr(VI) Removal Efficiency. It can be seen from Figure 7a that there is a significant interaction between $FeSO_4$ molarity and fly ash particle size on the Cr(VI) removal efficiency ($P = 0.0014 < 0.01$). The significant order is as follows: $FeSO_4$ molarity > particle size of fly ash. In the selected experimental range, the removal efficiency of Cr(VI) first increased and then decreased with the increase of $FeSO_4$ molarity and gradually decreased with the increase of fly ash particle size. It can be seen from Figure 7b that the interaction between $FeSO_4$ molarity and flow rate of $FeSO_4$ solution has no significant effect on the Cr (VI) removal efficiency ($P = 0.9166 > 0.05$), and the significant order is as follows: flow rate > $FeSO_4$ molarity. In the selected experimental range, the removal efficiency of Cr(VI) increased first and then decreased with the increase of $FeSO_4$ molarity and gradually increased with the increase of flow rate of $FeSO_4$ solution. It can be seen from Figure 7c that the interaction between fly ash particle size and flow rate of $FeSO_4$ solution has no significant effect on the Cr(VI) removal efficiency ($P = 0.1603 > 0.05$), and the significant order is as follows: flow rate > fly ash particle size. In the selected experimental range, the removal efficiency of Cr(VI) decreased with the increase of particle size and increased with the increase of flow rate of $FeSO_4$ solution.

3.3.2. Total Chromium Removal Efficiency. It can be seen from Figure 8a that the interaction between molarity of $FeSO_4$ and fly ash particle size has no significant effect on the total chromium removal efficiency ($P = 0.4317 > 0.05$), and the fly ash particle size is dominant among the two factors. In the selected experimental range, the removal efficiency of total chromium first increased and then decreased with the increase of $FeSO_4$ molarity and gradually decreased with the increase of

https://doi.org/10.1021/acsomega.2c03699
ACS Omega 2022, 7, 32331−32338

Table 5. Variance Analysis Table of Second-Order Model of Total Chromium Removal Efficiency

variance source	sum of squares	degree of freedom	Mean square	*F*-value	*p*-value
model	311.01	9	34.55	70.27	<0.0001
A-molarity of $FeSO_4$	58.32	1	58.32	118.60	<0.0001
B-the size of fly ash	135.87	1	135.87	276.33	<0.0001
C-the flow rate of $FeSO_4$ solution	56.33	1	56.33	114.57	<0.0001
AB	0.34	1	0.34	0.69	0.4317
AC	1.89	1	1.89	3.84	0.0907
BC	4.00	1	4.00	8.13	0.0246
A^2	38	1	38.30	77.88	<0.0001
B^2	3.25	1	3.25	6.61	0.0370
C^2	8.53	1	8.53	17.35	0.0042
residual error	3.44	7	0.49		
degree of misfit	3.44	3	1.15	52.13	0.0710
pure error	0.00088	4	0.00022		
total deviation	314.44	16			

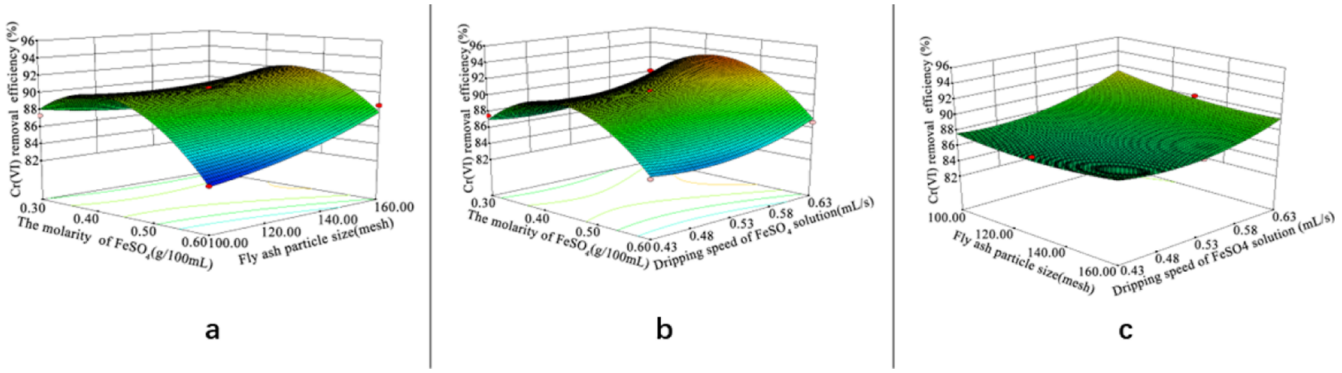

Figure 7. Response surface plot of Cr(VI) removal efficiency under the interaction of various factors. (a) Cr(VI) removal efficiency under the interaction of molarity of $FeSO_4$ and fly ash particle size. (b) Cr(VI) removal efficiency under the interaction of molarity of $FeSO_4$ and flow rate of $FeSO_4$ solution. (c) Cr(VI) removal efficiency under the interaction of flow rate of $FeSO_4$ solution and fly ash particle size.

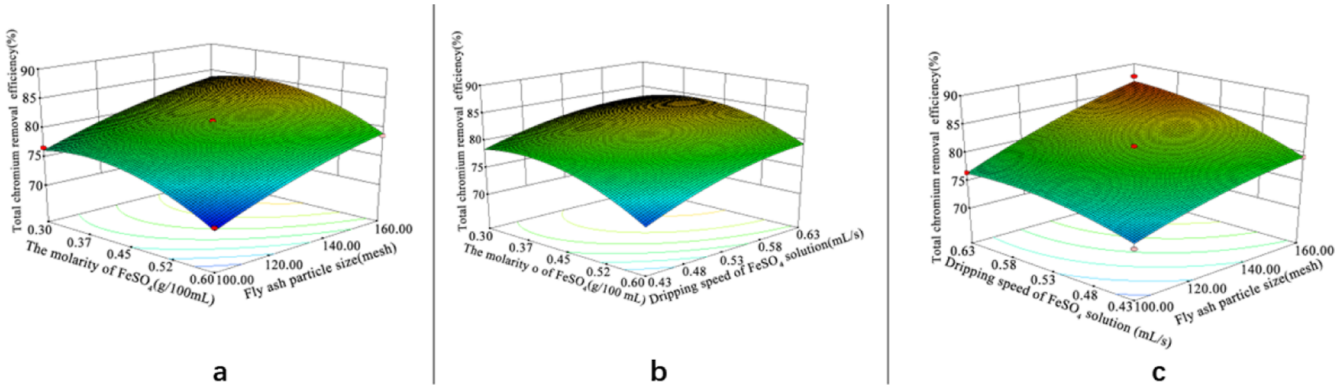

Figure 8. Response surface plot of total chromium removal efficiency under the interaction of various factors (a). Total chromium removal efficiency under the interaction of molarity of $FeSO_4$ and fly ash particle size. (b) Total chromium removal efficiency under the interaction of molarity of $FeSO_4$ and flow rate of $FeSO_4$ solution. (c) Total chromium removal efficiency under the interaction of flow rate of $FeSO_4$ solution and fly ash particle size.

fly ash particle size. It can be seen from Figure 8b that the interaction between molarity of $FeSO_4$ and flow rate of $FeSO_4$ solution has no significant effect on the total chromium removal efficiency ($P = 0.0907 > 0.05$), and the fly ash particle size is dominant among the two factors. In the selected experimental range, the removal efficiency of total chromium increased first and then decreased with the increase of $FeSO_4$ molarity and gradually increased with the increase of flow rate of $FeSO_4$ solution. It can be seen from Figure 8c that the interaction between fly ash particle size and flow rate of $FeSO_4$ solution has a significant impact on the total chromium removal efficiency ($P = 0.0246 < 0.05$), and the fly ash particle size is dominant among the two factors. In the selected experimental range, the removal efficiency of total chromium gradually decreased with the increase of particle size and gradually increased with the increase of dripping flow rate.

According to the experimental results of response surface, the optimum preparation conditions of nFeS-F were optimized by Design-Expert. The optimum preparation conditions of nFeS-F were as follows: the molarity of $FeSO_4$ is 0.45 mol/L,

https://doi.org/10.1021/acsomega.2c03699
ACS Omega 2022, 7, 32331−32338

the fly ash particle size is 120−150 mesh, and the flow rate of $FeSO_4$ solution is 0.43/100 mL.

Based on the experimental results of the response surface, the experimental conditions were optimized using Design-Expert, and the predicted optimal preparation conditions of nFeS-F were obtained as $FeSO_4$ concentration of 0.45 mol/L, fly ash particle size of 120−150 mesh, and flow rate of 0.43/100 mL. To confirm the accuracy of the predicted values, validation experiments were conducted under this preparation condition, and the results showed that the removal rates of Cr(VI) and total chromium were 92.87 and 83.53%, respectively. The difference between the model predicted values and the actual experimental values was within 10%,[32] which shows that the model can accurately simulate the influence of different factors on the removal efficiency of Cr(VI) and total chromium and has practical value.

4. CONCLUSIONS

In this study, a quadratic multiple regression equation (model) between fly ash particle size, $FeSO_4$ concentration, flow rate, and Cr(VI) and total chromium removal was developed based on the Box-Behnken experimental design method. Through 17 sets of fitting experiments, it was shown that the model fitted well with the experiments and the optimal preparation conditions of nFeS-F were obtained. nFeS-F, as an adsorbent material, can be used as a filler material for adsorption columns or permeable reaction walls and thus has some application value for the treatment of chromium in wastewater and contaminated water bodies. Detailed conclusions are as follows.

(1) Fly ash-loaded nano-FeS material was successfully prepared by the ultrasonic precipitation method, which realized the superposition of fly ash and nano-FeS on chromium removal ability, and gave full play to the efficient reduction ability of nano-FeS on Cr(VI) and effectively removed Cr(VI).

(2) The response surface method was used to establish the prediction models for the removal of Cr(VI) and total chromium, and the correlation coefficients of the models were 0.9629 and 0.9750, respectively, with good fit and small experimental errors, which could predict the effect of Cr(VI) and total chromium removal by nFeS-F prepared under different fly ash particle sizes, $FeSO_4$ material concentrations, and flow rates, respectively.

(3) The response surface model predicts that the optimal preparation conditions for nFeS-F are molarity of $FeSO_4$ of 0.45 mol/L, fly ash particle size of 120−150 mesh, and flow rate of 0.43 mL/s.

(4) The optimum preparation conditions resulted in 92.87 and 83.53% removal of Cr(VI) and total chromium, respectively. The differences between the model predicted values and the actual experimental values were within 10%, indicating that the model was accurate and reliable.

AUTHOR INFORMATION

Corresponding Author

Xuying Guo − *College of Mining and College of Science, Liaoning Technical University, Fuxin, Liaoning 123000, China;* orcid.org/0000-0002-2005-5418; Email: guoxuying@lntu.edu.cn

Authors

Zhiyong Hu − *College of Mining, Liaoning Technical University, Fuxin, Liaoning 123000, China*

Xinle Gao − *College of Mining, Liaoning Technical University, Fuxin, Liaoning 123000, China*

Yanrong Dong − *College of Civil Engineering, Liaoning Technical University, Fuxin, Liaoning 123000, China*

Saiou Fu − *College of Civil Engineering, Liaoning Technical University, Fuxin, Liaoning 123000, China*

Complete contact information is available at: https://pubs.acs.org/10.1021/acsomega.2c03699

Notes

The authors declare no competing financial interest.

ACKNOWLEDGMENTS

The project is funded by the National Natural Science Foundation of China (51304114), Department of Education of Liaoning Province (LJ2017FAL016 and LJKZ0340), "Double First-class" Innovation Team of Liaoning Technical University (LNTU20TD-21).

REFERENCES

(1) Yang, X.; Liu, L.; Zhang, M.; Tan, W.; Qiu, G.; Zheng, L. Improved removal capacity of magnetite for Cr (VI) by electrochemical reduction. *J. Hazard.* **2019**, *374*, 26−34.

(2) Korngold, E.; Belayev, N.; Aronov, L. Removal of chromates from drinking water by anion exchangers. *Sep. Purif. Technol.* **2003**, *33*, 179−187.

(3) Jiang, Y.; Liu, Z.; Zeng, G.; Liu, Y.; Shao, B.; Li, Z.; Liu, Q.; Zhang, W.; He, Q. Polyaniline-based adsorbents for removal of hexavalent chromium from aqueous solution: A mini review. *Environ. Sci. Pollut. Res.* **2018**, *25*, 6158−6174.

(4) Peng, H.; Guo, J. Removal of chromium from wastewater by membrane filtration, chemical precipitation, ion exchange, adsorption electrocoagulation, electrochemical reduction, electrodialysis, electrodeionization, photocatalysis and nanotechnology: a review. *Environ. Chem. Lett.* **2020**, *18*, 2055−2068.

(5) Gilhotra, V.; Yadav, R.; Sugha, A.; Das, L.; Vashisht, A.; Bhatti, R.; Bhatti, M. S. Electrochemical treatment of high strength chrome bathwater: A comparative study for best-operating conditions. *Clean. Eng. Technol.* **2021**, *2*, 100093.

(6) Busarev, A.; Abitov, S. A.; Selyugin, A. Chromium-containing wastewater treatment by means of using galvanocoagulators. *IOP Conf. Ser.: Mater. Sci. Eng.* **2020**, *890*, 012149.

(7) Du, J.; Shang, X.; Li, T.; Guan, Y. Recycling and modeling of chromium from sludge produced from magnetic flocculation treatment of chromium-containing wastewater. *Process Saf. Environ. Prot.* **2022**, *157*, 20−26.

(8) Fan, H.; Chen, Y.; Hu, Y. In-situ synthesis of Nano-FeS by sulfate reducting bacteria for Cr(VI) reduction. *Environ. Prot. Chem. Ind.* **2022**, *42*, 61−67.

(9) Li, Y.; Wang, W.; Zhou, L.; Liu, Y.; Mirza, Z. A.; Lin, X. Remediation of hexavalent chromium spiked soil by using synthesized iron sulfide particles. *Chemosphere* **2017**, *169*, 131−138.

(10) Liu, Y.; Xue, H.; Chen, J. Progress Research on Removal Effect of Heavy Metal Cr(VI) by Nano Zero-valent Iron. *Synth. Mater. Aging Appl.* **2019**, *48*, 154.

(11) Yao, Y.; Mi, N.; He, C.; Zhang, Y.; Yin, L.; Li, J.; Wang, L.; Yang, S.; He, H.; Li, S.; Ni, L. A novel colloid composited with polyacrylate and nano ferrous sulfide and its efficiency and mechanism of removal of Cr (VI) from Water. *J. Hazard. Mater.* **2020**, *399*, 123082.

(12) Park, M.; Park, J.; Kang, J.; Han, Y. S.; Jeong, H. Y. Removal of hexavalent chromium using mackinawite (FeS)-coated sand. *J. Hazard. Mater.* **2018**, *360*, 17−23.

(13) Guo, X.; Fu, S.; Dong, Y. Study on preparation of adsorption material (nano FeS loaded on lignite) and its chromium removal performance. *Coal Sci. Technol.* **2020**, *48*, 152−159.
(14) Jiang, L. Present situation and development suggestions of comprehensive utilization of fly ash in coal-fired power plants. *Clean Coal Technol.* **2020**, *26*, 31−39.
(15) Wang, N.; Sun, X.; Zhao, Q.; Yang, Y.; Wang, P. Leachability and adverse effects of coal fly ash: A review. *J. Hazard. Mater.* **2020**, *396*, 122725.
(16) Liu, J., Lu, X. Study on the treatment for chromium-containing wastewater by fly ash.*2011 International Conference on Electrical and Control Engineering*; IEEE, 2011; pp 1794−1797.
(17) Wang, N.; Jin, L.; Li, C.; Liang, Y.; Wang, P. Preparation of coal fly ash-based Fenton-like catalyst and its application for the treatment of organic wastewater under microwave assistance. *J. Clean. Prod.* **2022**, *342*, 130926.
(18) Wang, N.; Sun, X.; Zhao, Q.; Wang, P. Treatment of polymer-flooding wastewater by a modified coal fly ash-catalysed Fenton-like process with microwave pre-enhancement: System parameters, kinetics, and proposed mechanism. *Chem. Eng. J.* **2021**, *406*, 126734.
(19) Ribeiro, P. B.; de Freitas, V. O.; Machry, K.; Muniz, A. R. C.; da Rosa, G. S. Evaluation of the potential of coal fly ash produced by gasification as hexavalent chromium adsorbent. *Environ. Sci. Pollut. Res.* **2019**, *26*, 28603−28613.
(20) Wang, J.; Zhang, J.; Yang, Q. Adsorption characteristics of Fly ash for Cr (VI). *Chin. J. Environ. Eng.* **2014**, *8*, 4593−4599.
(21) Li, X.; Zhao, X.; Xiang, Y. Experimental Study on Adsorption Cr(III) and Cr (VI) of Chromium-containing Wastewater by Modified Fly Ash. *Non-Met. Mines.* **2015**, *38*, 75.
(22) Chen, Z.; Iron-Based Nanomaterials Preparation and Its Removal Mechanism for Uranium and Chromium in Water. North China Electric Power University: Beijing, 2020.
(23) Bose, B., Mukherjee, T., Rahaman, R. Simultaneous adsorption of manganese and fluoride from aqueous solution via bimetal impregnated activated carbon derived from waste tire: Response surface method modeling approach, *Environ. Prog. Sustain. Energy*, **2021**, *40* ().DOI: DOI: 10.1002/ep.13600
(24) Dai, Z.; Liu, S.; Bao, J.; Ju, H. Nanostructured FeS as a mimic peroxidase for biocatalysis and biosensing. *Chem.—Eur. J.* **2009**, *15*, 4321−4326.
(25) Liang, G.; Li, Y.; Yang, C.; Zi, C.; Zhang, Y.; Hu, X.; Zhao, W. Production of biosilica nanoparticles from biomass power plant fly ash. *Waste Manag.* **2020**, *105*, 8−17.
(26) Zeng, T., Haidu, N., Haichao, S. H. Performance and mechanism of Cr (VI) removal by sludge-derived biochar loaded with nanoscale zero-valent iron. *Acta Mater. Compos. Sin.* **2022**, *40*, 1−13.
(27) Xu, H.; Li, F.; Chen, S. Precipitation Process of Nanometer Particles Chemical Principles and Effects of Operation Parameters. *Chem. Ind. Eng. Prog.* **1996**, 29.
(28) Luo, P.; Nieh, T. G.; Schwartz, A. J.; Lenk, T. J. Surface characterization of nanostructured metal and ceramic particles. *Mater. Sci. Eng. A* **1995**, *204*, 59−64.
(29) Madureira, J.; Melgar, B.; Santos-Buelga, C.; Margaça, F. M.; Ferreira, I. C.; Barros, L.; Verde, S. C. Phenolic compounds from irradiated olive wastes: Optimization of the heat-assisted extraction using response surface methodology. *Chemosensors* **2021**, *9*, 231.
(30) Khelifi, O.; Affoune, A. M.; Nacef, M.; Chelaghmia, M. L.; Laksaci, H. Response surface modeling and optimization of Ni (II) and Cu (II) ions competitive adsorption capacity by sewage sludge activated carbon. *Arabian J. Sci. Eng.* **2021**, *47*, 5797.
(31) Ayele, A.; Suresh, A.; Benor, S.; Konwarh, R. Optimization of chromium (VI) removal by indigenous microalga (Chlamydomonas sp.)-based biosorbent using response surface methodology. *Water Environ. Res.* **2021**, *93*, 1276−1288.
(32) Zhou, R.; Zhang, M.; Li, J.; Zhao, W. Optimization of preparation conditions for biochar derived from water hyacinth by using response surface methodology (RSM) and its application in Pb^{2+} removal. *J. Environ. Chem. Eng.* **2020**, *8*, 104198.

https://doi.org/10.1021/acsomega.2c03699
ACS Omega 2022, 7, 32331−32338